

**High Performance, High Temperature Piezoelectric Crystals
BiB3O6**

Journal:	<i>Journal of Materials Chemistry C</i>
Manuscript ID:	TC-ART-09-2014-002112.R1
Article Type:	Paper
Date Submitted by the Author:	15-Oct-2014
Complete List of Authors:	Yu, Fapeng; Institute of Crystal Materials and State Key Lab. of Crystal Materials, Shandong University Lu, Qingming; School of Chemistry and Chemical Engineering, Zhang, Shujun; Materials research Institute, Pennsalvina State University Cheng, Xiufeng; Shandong University, State Key Laboratory of Crystal Materials Wang, Hwei; Institute of Crystal Materials and State Key Lab. of Crystal Materials, Zhao, Xian; Shandong University, State Key Laboratory of Crystal Materials

ARTICLE

High Performance, High Temperature Piezoelectric Crystals BiB_3O_6

Cite this: DOI: 10.1039/x0xx00000x

Fapeng Yu ^{a, d}, Qingming Lu ^b, Shujun Zhang ^c, Hwei Wang ^a, Xiufeng Cheng ^a and Xian Zhao ^a,

Received 00th January 2012,
Accepted 00th January 2012

DOI: 10.1039/x0xx00000x

www.rsc.org/

High performance piezoelectric materials are desirable for piezoelectric sensing applications. In this paper, piezoelectric crystals, α - BiB_3O_6 (BIBO), were explored for high temperature sensing. Dielectric, piezoelectric and electromechanical properties were evaluated by using the impedance method, where the piezoelectric charge coefficients were determined to be on the order of d_{14} =10.9, d_{16} =13.9, d_{21} =16.7, d_{22} =40.0, d_{23} =2.5, d_{25} =4.3, d_{34} =18.7 and d_{36} =13.0 pC/N, with corresponding piezoelectric voltage coefficients g_{14} =122, g_{16} =144, g_{21} =225, g_{22} =538, g_{23} =34, g_{25} =58, g_{34} =165 and g_{36} =121 $\times 10^{-3}$ V·m/N at room temperature (RT). Of particular significance is that the receiving sensitivity of BIBO crystals was found to be on the order of 47.2 pm²/N, nearly one order higher than that of LiNbO_3 crystals. Moreover, the BIBO crystals were found to possess high mechanical quality factor Q_m (13000 at RT and >1000 at 600°C), low dielectric loss (<0.1% at RT and 15% at 600°C and 1kHz), high electrical resistivity ($\sim 2.5 \times 10^8$ Ω ·cm at 600°C) and high temperature stability of piezoelectric coefficients (variations $\leq \pm 10\%$). All these properties demonstrate BIBO crystals are promising for piezoelectric sensing over a broad temperature range.

A. Introduction

Since the discovery of piezoelectric effect in 1880, various piezoelectric devices have been designed and fabricated, such as resonators, filters, transducers, actuators and sensors etc. As the development of science and technology, high temperature piezoelectric sensors are desirable in many fields, where piezoelectric materials operated at elevated temperatures without failure are in demand for the structural health monitoring, non-destructive evaluation and oil exploration industries etc. [1-5].

From application point of view, the operational temperature range of the smart transducers is limited by the sensing capability of piezoelectric materials at elevated temperatures, increased conductivity and mechanical attenuation, and variation of the piezoelectric properties with temperature [1]. Therefore, high performance piezoelectric materials with the merits of large piezoelectric coefficient and electromechanical coupling factor, high electrical resistivity, low dielectric loss, and high temperature stability of electro-elastic properties are desired for sensor design and fabrications.

Of all the currently commercialized piezoelectric materials (including the lead-based ferroelectric (ferro.) ceramics and single crystals, and non-ferroelectric (non-ferro.) piezoelectric single crystals, as listed in Table I), the lead-based ferroelectric materials with the perovskite structure ABO_3 , such as $\text{Pb}(\text{Zr,Ti})\text{O}_3$ (PZT) ceramics and $\text{Pb}(\text{Mg}_{1/3}\text{Nb}_{2/3})\text{O}_3$ - PbTiO_3

(PMN-PT) single crystals, offer high piezoelectric coefficients and electromechanical coupling factors, but inferior temperature stability and low temperature usage range, being limited by their respective Curie points (160-350°C) or polymorphic phase transition temperatures [6,7]. Comparing to the perovskite ferroelectrics, the non-ferroelectric langasite, GaPO_4 and $\text{ReCa}_4\text{O}(\text{BO}_3)_3$ (Re: rare-earth elements) piezoelectric crystals were reported to possess low piezoelectric coefficients, 2-3 orders of magnitude lower than those of perovskite ferroelectric materials, but exhibit higher mechanical quality factor Q_m , lower dielectric loss, and broader operational temperature range (Table I), revealing their potentials for high temperature resonance/non-resonance based piezoelectric sensor applications. Of particular interest is that the non-ferroelectric piezoelectric α - BiB_3O_6 (BIBO) crystals were reported to exhibit attractive piezoelectric properties, with large longitudinal piezoelectric coefficient d_{22} being on the order of -39.5 pC/N at room temperature [8], double the value of commercialized LiNbO_3 (LN) ferroelectric crystals (d_{22} =21 pC/N [9]), and 5-8 times that of langasite crystals (d_{11} =~7 pC/N [10]), potential for high temperature piezoelectric applications.

The BiB_3O_6 is a binary compound. Since the discovery of α - BiB_3O_6 in 1962 [11], considerable attention has been paid to the synthesis of new compounds from Bi_2O_3 and B_2O_3 components [12-17]. Up to now, there are four BiB_3O_6 polymorphs have been identified, i.e. α -, β -, γ - and δ - BiB_3O_6 , where the α - and δ - BiB_3O_6 crystals, belonging to monoclinic ($C2$) and orthorhombic ($Pca2_1$)

crystal symmetries, respectively, were found to show the noncentrosymmetric characteristics and exhibit stable temperature regions around 710-715°C and 680-710°C, respectively [17]. In the past two decades, extensive studies have been carried out on the crystal growth, structure, and optical properties of α - and δ -BiB₃O₆ crystals for nonlinear optical applications [15-20]. However, investigations of the electro-elastic properties for piezoelectric

applications are very limited [8, 17]. In this research, α -BiB₃O₆ crystals were explored for high temperature piezoelectric sensor applications. Dielectric, elastic and piezoelectric properties were evaluated by the impedance method. Moreover, temperature dependent behaviours of dielectric and piezoelectric properties were investigated in the temperature range of 20-600°C, and the properties were compared with commercialized LN crystals.

Table I Properties of different piezoelectric materials, including perovskite ferroelectrics and non-ferroelectric piezoelectric materials.

Materials	T_c/T_0 (°C)	ϵ^T/ϵ^0	$\tan\delta$	k_t (%)	d_{33} (pC/N) *	Q_m	Ferro./Non-ferro.
PZT [6]	193	3400	2%	75	600	75	Ferro.
PMN-PT [7]	155	8200	0.4%	95	2800	100	Ferro.
Quartz [21]	~573	4.5	<0.01%	<8	~2	>10000	Non-ferro.
LiNbO ₃ [9]	~1170	84	<0.1%	~35	~21	>10000	Ferro.
LGX [10]*	1300-1500	16-80	<0.5%	16	~7	~10000	Non-ferro.
ReCOB [1, 22, 23]	1400-1510	9-11	<0.1%	6-8	2~3	~10000	Non-ferro.
GaPO ₄ [24]	970	6-7	<0.1%	-	4.5	>10000	Non-ferro
Ba ₂ TiSi ₂ O ₈ [25]	1445	10-17	<0.1%	16.2	4	-	Non-ferro
Ca ₂ Al ₂ SiO ₇ [26]	~1600	10-11	-	-	-	-	Non-ferro
BiBO [8]	726	8-9	-	-	39.5	-	Non-ferro.

*LGX: Languisite type crystals including the crystals with ordered and disordered structures; d_{33} is the longitudinal piezoelectric coefficient, here including the d_{11} , d_{22} and d_{33} .

B. Experimental

2.1 Crystal growth and orientation. The BIBO single crystals were grown by the conventional top-seeded solution method. Raw materials, Bi₂O₃ and H₃BO₃ with 4N purity, were weighed according to the stoichiometric ratio, and fully mixed for more than 10 hrs, then pressed into tablets and sintered at 600°C for at least 20 hrs to get the polycrystalline BIBO compounds. The synthesized polycrystalline compounds were charged into the Pt crucible and then heated about 120°C higher than the observed melting point for >24 hrs to make the melt uniform enough for single crystal growth. The growth period was controlled to be ~3 months and the cooling region was selected to be ~3°C during the crystal growth. Figure 1 gives the as-grown BIBO crystal along the $[\bar{1}01]$ orientation, with strong habitual facets, relating to the monoclinic symmetry (point group 2).

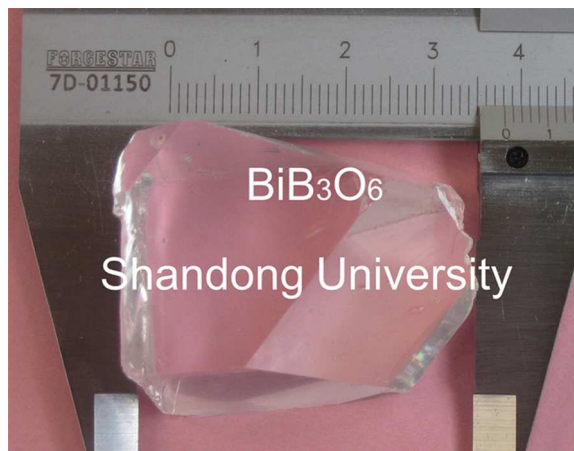


Figure 1 As-grown BIBO single crystal by the top-seeded solution method

It is worthy to mention that there are two kinds of BIBO crystals, namely left- (laevorotatory) and right-hand

(dextrorotatory) BIBO crystals, due to the crystal symmetry of point group 2. The left- and right-hand BIBO crystals can be recognized from well-developed morphology [8], where the direction of positive crystallographic b -axis corresponds to the piezoelectric Y -axis with piezoelectric coefficient d_{22} being negative for the left-hand BIBO crystals, while the positive b -axis is identical to positive Y -axis with piezoelectric d_{22} being positive for the right-hand BIBO crystals, as shown in Figure 2(b). In this study, all the crystal cuts were prepared from right-hand BIBO crystals.

For electro-elastic properties evaluation, the relationship between crystallographic axes and physical axes for BIBO crystals was determined based on the IEEE Standard on Piezoelectricity [27], where the physical Y - and Z -axes are parallel to the crystallographic b - and c -axes, respectively, while the X -axis is perpendicular to the YZ plane to form the right-hand orthogonal system. Based on the cell parameters determined for BIBO crystals ($a=7.116$, $b=4.993$, $c=6.508$, $\alpha=\gamma=90.0^\circ$, and $\beta=105.6^\circ$) [8], the angle between the physical X -axis and crystallographic a -axis was obtained and determined to be on the order of 15.6° . Figure 2 gives the relationship between the crystallographic axes and physical axes for right-hand (dextrorotatory) BIBO piezoelectric crystals.

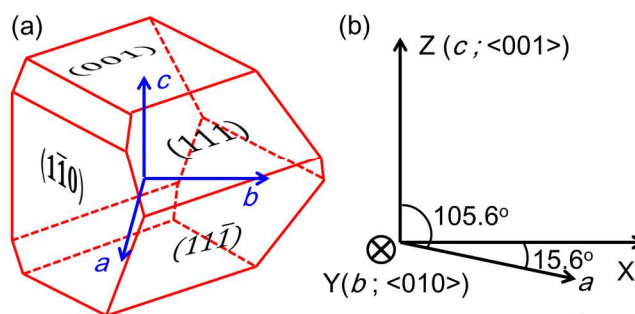


Figure 2 Morphology of BIBO crystal grown along $[\bar{1}01]$ direction and the habitual faces (a); the relationships between the crystallographic axes and physical axes for the right-hand BIBO crystals (b)

2.2 Sample preparation and electro-elastic constants evaluation.

Restricted by the crystal symmetry, BIBO piezoelectric crystals possess 25 independent material constants, including 4 dielectric permittivities, 8 piezoelectric coefficients and 13 elastic constants, which are given below,

$$\varepsilon_{ij} = \begin{pmatrix} \varepsilon_{11} & 0 & \varepsilon_{13} \\ 0 & \varepsilon_{22} & 0 \\ \varepsilon_{13} & 0 & \varepsilon_{33} \end{pmatrix}$$

$$d_{ij} = \begin{pmatrix} 0 & 0 & 0 & d_{14} & 0 & d_{16} \\ d_{21} & d_{22} & d_{23} & 0 & d_{25} & 0 \\ 0 & 0 & 0 & d_{34} & 0 & d_{36} \end{pmatrix}$$

$$s_{ij} = \begin{pmatrix} s_{11} & s_{12} & s_{13} & 0 & s_{15} & 0 \\ s_{12} & s_{22} & s_{23} & 0 & s_{25} & 0 \\ s_{13} & s_{23} & s_{33} & 0 & s_{35} & 0 \\ 0 & 0 & 0 & s_{44} & 0 & s_{46} \\ s_{15} & s_{25} & s_{35} & 0 & s_{55} & 0 \\ 0 & 0 & 0 & s_{46} & 0 & s_{66} \end{pmatrix}$$

All these electro-elastic constants were evaluated by measuring the capacitance, resonance and anti-resonance frequencies of different crystal cuts designed in Figure 3, using a multi-frequency LCR meter (Agilent 4263B) and Impedance-Phase Gain Analyzer HP4194A.

The BIBO piezoelectric crystals were orientated by using an X-ray diffraction crystal direction finder (YX-4 made by China Liaodong Radioactive Instrument Co.Ltd) with accuracy of $<20''$, and the crystal cuts were prepared by using a precise inner diameter saw (JCY5060, China), with accuracy of $\pm 0.01\text{mm}$. The dimensional ratios of the prepared crystal cuts were ranged from 1:6:6 to 1:8:8 for square plates (samples (d, e, f and n)), 1:1:2.5 to 1:1:3 for rod samples (sample (c)), and 1:2.5:8 to 1:3.5:10 for rectangular samples (samples (a, b, g, h, i, j, k, l, m, o, and p)).

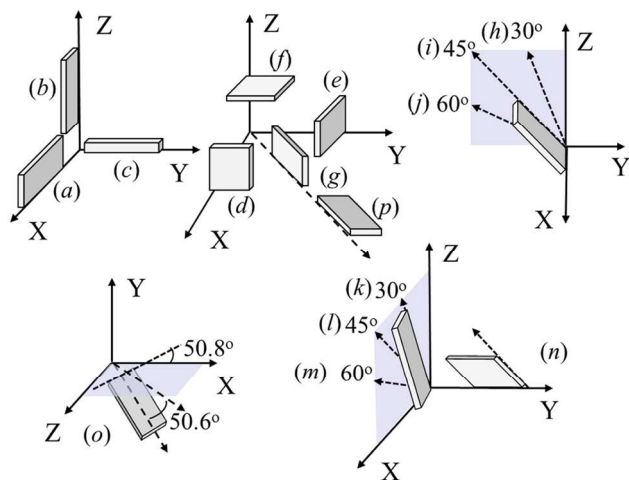


Figure 3 Different crystal cuts for electro-elastic constants evaluations [(a) YX plate, (b) YZ plate, (c) Y-rod, (d) X square plate, (e) Y square plate, (f) Z square plate, (g) (YXw)36.1°, (h) (YZw)30° cut, (i) (YZw)45° cut, (j) (YZw)60° cut, (k) (YZt)30° cut, (l) (YZt)45° cut, (m) (YZt)60°, (n) (ZXw)-45° square plate, (o) (YZtw)50.8°/50.6°, and (p) (ZXt)36.1°]

Table II Summarized the crystal cuts and vibration modes for determining the electro-elastic constants of BIBO crystals. Different to the determination scheme reported by Mason for crystals in point group 2 [28], we established improved determination scheme for the BIBO crystals. All the 25 independent electro-elastic constants were obtained by measuring the longitudinal (length extension and thickness extension), transverse (length extension), and shear vibration modes (face shear and thickness shear) of 16 different crystal cuts. The piezoelectric charge coefficients d_{ij} and piezoelectric voltage coefficients g_{ij} were evaluated by using the following equations,

$$d_{ij} = k_{ij}(\varepsilon_{ii}s_{jj})^{1/2} \quad (1)$$

$$g_{ij} = d_{ij} / \varepsilon_{ij} \quad (2)$$

where k_{ij} , ε_{ii} and s_{jj} are electromechanical coupling factor, dielectric permittivity and elastic compliance, respectively. In addition, the mechanical quality factor Q_m is evaluated by using equation (3), based on the Butterworth-Van Dyke equivalent circuit, where R_s and C_s are the series components of the equivalent circuit and have the physical meaning of motional resistance and capacitance.

$$Q_m = \frac{1}{2\pi f_r R_s C_s} \quad (3)$$

Table II Summary of the crystal cuts and vibration modes for electro-elastic constants determination in point group 2.

Crystal cuts	Modes*	Material constants
X-plate (d)		ε_{11}
Y-plate (e)		ε_{22}
Z-plate (f)		ε_{33}
(YZw)45° (i)		$\varepsilon_{13} (\varepsilon_{33}' = 0.5\varepsilon_{33} + \varepsilon_{13} + 0.5\varepsilon_{11})$
Y-rod (c)	LLE	s_{22}, d_{22}
Y-plate (e)	TE	$d_{33}' = d_{22} (d_{33} \text{ meter})$
	FS	s_{55}, d_{25}
X-plate (d)	FS	s_{44}, d_{14}
	TS	s_{66}, d_{16}
Z-plate (f)	FS	s_{66}, d_{36}
	TS	s_{44}, d_{34}
YX plate (a)	TLE	s_{11}, d_{21}
YZ plate (b)	TLE	s_{33}, d_{23}
(YZw)30° (h)		s_{23}
(YZw)45° (i)	TLE	$[s_{33}'(\alpha) = s_{22}\sin^4\alpha + s_{33}\cos^4\alpha + (2s_{23} + s_{44})\sin^2\alpha\cos^2\alpha]$
(YZw)60° (j)		$\sin^2\alpha\cos^2\alpha$
(YZt) 30° (k)		s_{13}, s_{15}, s_{35}
(YZt)45° (l)	TLE	$[s_{33}'(\beta) = s_{11}\sin^4\beta + (2s_{13} + s_{55})\sin^2\beta\cos^2\beta + s_{15}\sin^3\beta\cos\beta + 2s_{35}\cos^3\beta\sin\beta + s_{33}\cos^4\beta]$
(YZt)60° (m)		
(YXw)36° (g)	TLE	$s_{12} [s_{11}' = 0.428s_{11} + 0.226(s_{66} + 2s_{12}) + 0.119s_{22}]$
(ZXt)36° (p)		
(ZXw)-45° (n)	FS	$s_{46} (s_{66}' = 0.5s_{44} - s_{46} + 0.5s_{66})$
(YZtw)50.8° / 50.6° (o)	TLE	$s_{23} (s_{33}' = 0.058s_{11} + 0.289s_{12} + 0.078s_{13} + 0.095s_{15} + 0.357s_{22} + 0.193s_{23} + 0.236s_{25} + 0.026s_{33} + 0.063s_{35} + 0.096s_{44} + 0.236s_{46} + 0.039s_{55} + 0.145s_{66})$

* LLE: longitudinal length extensional vibration mode; TE: thickness extensional vibration mode; TLE: transverse length extensional vibration mode; FS: face shear vibration mode; TS: thickness shear vibration mode; α and β are the rotation angles around physical X- and Y- axes, respectively.

2.3 Electrical resistivity and temperature dependence of electro-elastic constants. The electrical resistivities were obtained by measuring the currents of X-, Y- and Z-plates at 100V, using a source meter (Keithley 2410C). For electro-elastic constants evaluation, the capacitance, resonance and anti-resonance frequencies of crystal cuts at elevated temperatures were measured using a multi-frequency LCR meter (Agilent 4263B) and Impedance-Phase Gain Analyzer HP4194A, connected to a special designed high temperature furnace, where the temperature was precisely controlled from room temperature to 600°C.

C. Results and discussions

3.1 Microstructure. The BIBO crystals consist of borate sheets, built by corner-shearing $[\text{BO}_3]$ and $[\text{BO}_4]$ groups, connected by Bi^{3+} cations (Figures 4(a) and 4(b)), forming B(1)-O tetrahedrons, B(2)-O trigons and distorted Bi-O octahedrons [29], exhibiting layered structure characteristics. The Bi-O octahedrons are linked by four O(3) atoms, which are shared by three B(2)-O trigons, while the left two O(2) atoms in Bi-O octahedron are linked by B(1)-O tetrahedron and B(2)-O trigon. Meanwhile, the B(1)-O tetrahedron and B(2)-O trigon are connected to each other by O(1) atom, forming three dimensional network, as shown in Figures 4(c) and 4(d). The bonds formed in BIBO crystals (Bi-O and B-O bonds) are predominantly covalent, judged by the electrical negativity χ ($\chi_{\text{B}}=2.04$ eV, $\chi_{\text{Bi}}=2.02$ eV and $\chi_{\text{O}}=3.44$ eV). For the Bi-O octahedron, the d^{10} metal Bi^{3+} cation is bonded with ambient six O atoms, leaving nonbonding lone-pair electrons ($6s^2$ electrons), contributing to the distorted Bi-O octahedron. It is noticed that the average bond length of Bi-O (2.373Å) in BIBO crystals is longer than those of B-O bonds (1.462 Å for B(1)-O bond and 1.375 Å for B(2)-O bond) (Table III), the longer covalent bonds of Bi-O between the layers show the weaker bond strength, while the shorter covalent bonds of B-O inside the layers show stronger bond strength. According to the Jahn-Teller

effect on polyhedrons [30-32], the magnitudes of out-of-center distortions (Δd) for Bi-O octahedron and B-O tetrahedron were calculated and found to be on the order of 1.56 Å and 0.29 Å, respectively (Table III), demonstrating a strong anisotropic characteristic. The distorted Bi-O octahedron (strong distortion $\Delta d=1.56$ Å) and B-O tetrahedron (moderate distortion $\Delta d=0.29$ Å) are believed to account for the anisotropic thermal and electrical properties.

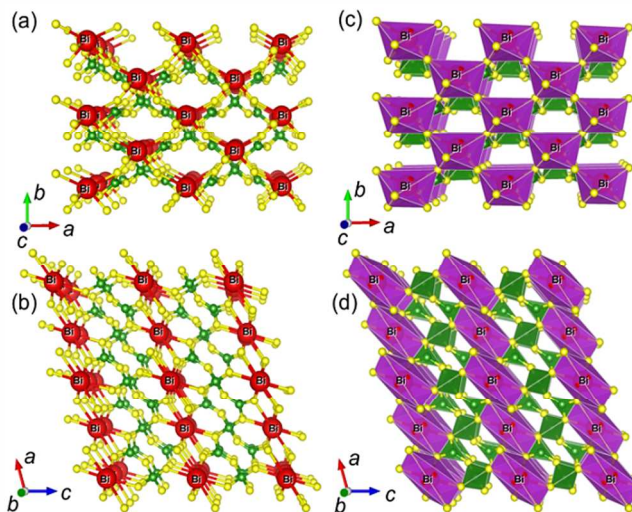


Figure 4 Structure fragments of the monoclinic BIBO crystals (perspective views along crystallographic c -axis (a) and b -axis (b) in space; (c) projected along the crystallographic c -axis, and (d) projected along the crystallographic b -axis in space. Structure data are referred to the ICSD, no. 48025)

Table III The atomic distance (bond length) in BIBO unit cell (refer to ICSD, no. 48025).

Configurations	Bonds	Bond length	Average bond length	Pauling bond strength	Distortion Δd
Bi-O octahedron	Bi-O(2)	2.390 Å	2.373 Å	0.5	1.56 Å
	Bi-O(3)	2.095 Å			
	Bi-O(3)'	2.633 Å			
B-O tetrahedron	B(1)-O(1)	1.436 Å	1.457 Å	0.75	0.29 Å
	B(1)-O(2)	1.478 Å			
	B(2)-O(1)	1.339 Å			
B-O trigon	B(2)-O(2)	1.411 Å	1.375 Å	1.0	-
	B(2)-O(3)	1.374 Å			

3.2 Electro-elastic constants. The full set of the dielectric, elastic and piezoelectric constants for BIBO crystals were determined and the results are summarized in Table IV, with reported data for comparison. It is interesting to note that the BIBO crystals possess strong piezoelectric properties. Of all the eight independent piezoelectric coefficients for BIBO crystals, the longitudinal charge coefficient d_{22} was determined to be the largest, being on the order of 40.0 pC/N, double the value of the LN crystals ($d_{22} = \sim 21$ pC/N). In addition, the piezoelectric voltage coefficients g_{22} was found to be on the order of $538 \times 10^{-3} \text{ V} \cdot \text{m/N}$ at RT, more than one order higher than that of LN crystals ($g_{22} = 29 \times 10^{-3} \text{ V} \cdot \text{m/N}$ [33]).

It is needed to point out that the opposite sign of the piezoelectric coefficients reported in ref. 8 were associated with the left-hand BIBO crystals, according to the IEEE standard [27]. For

verification of the determined piezoelectric coefficients, orientation dependence of the piezoelectric coefficients, including the longitudinal piezoelectric d_{22} , length extensional piezoelectric d_{13} , d_{21} and d_{23} , and shear piezoelectric d_{36} were investigated based on the determined piezoelectric coefficients (Table IV) using equations (4-8) (α , β and γ are the rotation angles around physical X-, Y- and Z-axes, respectively), results are given in Figure 5, together with the measured values for comparison. The good agreement of the calculated and measured values indicates the validity of the determined piezoelectric coefficients.

$$d'_{13} = -d_{14} \sin \alpha \cos \alpha \quad (4)$$

$$d'_{21} = d_{21} \cos^3 \gamma + (d_{22} - d_{16}) \sin^2 \gamma \cos \gamma \quad (5)$$

$$d'_{23} = d_{23} \cos^2 \beta + d_{21} \sin^2 \beta + d_{25} \sin \beta \cos \beta \quad (6)$$

$$d'_{22} = d_{22} \cos^3 \alpha + (d_{23} + d_{34}) \sin^2 \alpha \cos \alpha \quad (7) \quad d'_{36} = d_{36} \cos^2 \beta - d_{14} \sin^2 \beta + (d_{16} - d_{34}) \sin \beta \cos \beta \quad (8)$$

Table IV Electro-elastic constants of the monoclinic BIBO piezoelectric crystals

Elastic compliances s_{ij}^E (pm ² /N)													
	s_{11}	s_{12}	s_{13}	s_{15}	s_{22}	s_{23}	s_{25}	s_{33}	s_{35}	s_{44}	s_{46}	s_{55}	s_{66}
BIBO	36.2	-48.0	2.9	17.9	85.0	-2.6	-23.8	10.2	9.3	65.0	11.5	26.5	19.1
BIBO ^a	34.25	-46.75	-0.03	20.09	83.18	-1.27	-27.56	7.33	6.87	55.16	15.34	31.72	19.21
Elastic stiffness c_{ij}^E (10 ¹⁰ N/m ²)													
	c_{11}	c_{12}	c_{13}	c_{15}	c_{22}	c_{23}	c_{25}	c_{33}	c_{35}	c_{44}	c_{46}	c_{55}	c_{66}
BIBO	12.4	6.1	1.0	-3.2	4.7	-0.9	0.4	15.7	-7.0	1.7	-1.0	8.8	5.9
BIBO ^a	15.97	7.42	6.00	-4.97	5.25	1.34	-0.43	20.52	-7.08	2.33	-1.86	7.46	6.69
Relative dielectric permittivities $\epsilon_{ij}^T/\epsilon^0$													
	ϵ_{11}	ϵ_{13}	ϵ_{22}	ϵ_{33}									
BIBO	12.0	-1.4	8.4	13.8									
BIBO ^a	12.35	-2.94	8.02	13.95									
Piezoelectric charge coefficients d_{ij} (pC/N)													
	d_{14}	d_{16}	d_{21}	d_{22}	d_{23}	d_{25}	d_{34}	d_{36}					
BIBO	10.9	13.9	16.7	40.0	2.5	4.3	18.7	13.0					
BIBO ^a	-6.8	-8.4	15.6	-39.5	-3.8	5.1	-16.3	-6.2					
Piezoelectric voltage coefficients g_{ij} (10 ⁻³ V·m/N)													
	g_{14}	g_{16}	g_{21}	g_{22}	g_{23}	g_{25}	g_{34}	g_{36}					
BIBO	122	144	225	538	34	58	165	121					
BIBO ^a	-99	-94	220	-557	-54	72	-153	-70					
Electromechanical coupling factor k_{ij} (%)													
	k_{14}	k_{16}	k_{21}	k_{22}	k_{23}	k_{25}	k_{34}	k_{36}					
BIBO	13.1	30.9	32.1	50.0	9.2	9.6	21.0	26.9					

Data (a) was from left-hand BIBO crystals [8]; g_{ij} values for BIBO^a were calculated based on the reported parameters.

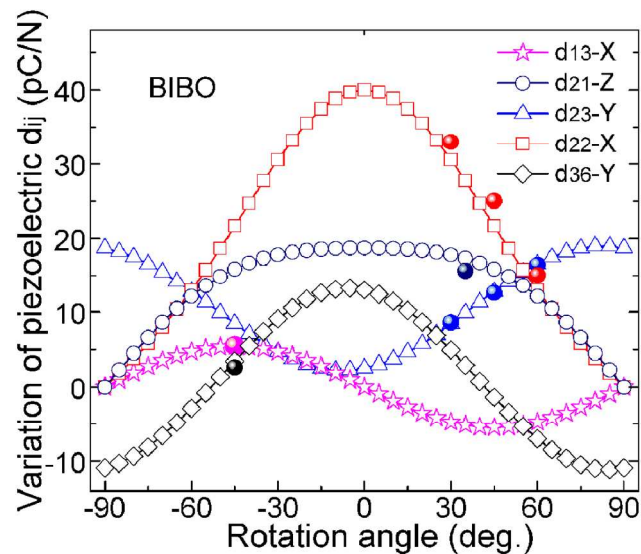


Figure 5 Variations of different piezoelectric coefficients as function of rotation angle around X-, Y- or Z-axes (the calculated values are given in open symbols and the measured values are shown in solid symbols).

3.3 Structure-property relationships.

3.3.1. Dielectric and elastic properties. The BIBO crystals were found to possess low dielectric permittivities being on the order of 12.0, 8.4 and 13.8 for $\epsilon_{11}^T/\epsilon^0$, $\epsilon_{22}^T/\epsilon^0$ and $\epsilon_{33}^T/\epsilon^0$ at RT, respectively. The dielectric permittivity is closely associated with the polarization of cations and anions in BIBO crystals, related to the electron polarization (derivation of the electron cloud, especially from the

lone pair electrons) and ionic polarization (relative motions of cations and anions) under electric field (the Bi-O octahedrons, B(1)-O tetrahedrons and B(2)-O trigons all contribute to the polarizations [34], here we just discuss the Bi-O octahedrons, due to their strong distortion and lone-pair electrons of Bi³⁺) [35].

Considering the characteristics of covalent bonds of Bi-O in BIBO crystals, the macroscopic polarizability α_M , which is relevant to the macroscopic dielectric permittivity, is mainly attributed to the electronic component polarizability (α_e) and ionic component polarization (α_i), where α_e is predominant. It is obtained from the crystal structure (Figures 4(c) and 4(d)) that the average bond lengths of Bi-O along the crystallographic *a*-axis (2.4235 Å) and *c*-axis (2.3204 Å) are higher than that along *b*-axis (1.249 Å), thus it is reasonable to presume that the orbital electrons of Bi³⁺ are easy to deviate from the nucleus along *a*- and *c*-axis than along *b*-axis under electrical field, leading to relatively larger magnitude of α_e along *a*- and *c*-axes than *b*-axis, which can be confirmed by the measured crystal refractivity n_i ($n_b < n_a$ and $n_b < n_c$ [36]). The refractivity n_i relates to the relative dielectric permittivity ϵ_r (by equation (9)), where c is the speed of light in vacuum and v is the velocity of light in the crystal.

$$n_i = \frac{c}{v} = \sqrt{\epsilon_r} \quad (9)$$

Besides, the special crystal structure (distorted Bi-O octahedrons with average bond lengths along *a*- and *c*-axes longer than that along *b*-axis) also affects the relative motions of cations and anions under electric field (ionic polarization), leading to a smaller magnitude of α_i value along *b*-axis than those along *a*- and *c*-axes. Thus, the anisotropy of the electronic polarizability α_e and ionic polarization α_i contributes to the low dielectric permittivity $\epsilon_{22}^T/\epsilon^0$.

Similar to the dielectric permittivity, the elastic stiffness (and compliance) also show large anisotropy along the physical X-, Y-

and Z-axes, with stiffness constants $c_{33} > c_{11} > c_{22}$, as given in Table IV. It is observed that the BIBO crystals possess layered structure normal to the (001) plane, however, the elastic stiffness along crystallographic c -axis was found to be the highest, different from the reported crystals with layered structure [25]. This phenomenon is closely related to the crystal bonding. It is believed that albeit the distance between the adjacent Bi^{3+} cations along the crystallographic c -axis ($d=6.508 \text{ \AA}$) is larger than that along the b -axis (4.993 \AA), the strong B-O bonds approximately along the c -axis (inclination angle between B-O trigon and c -axis is $\sim 30^\circ$) reinforced the bonding along the c -axis, contribute to the relative high elastic stiffness c_{33} , the similar case for the stiffness c_{11} (inclination angle between B-O trigon and c -axis is $\sim 35^\circ$), while the low stiffness c_{22} is owing to the relatively weak effective bond strength along b -axis, which can be confirmed by the thermal expansions, where BIBO shows the largest thermal expansion coefficient along Y-axis ($\alpha_{11}=7.3 \times 10^{-6}/^\circ\text{C}$, $\alpha_{22}=44.1 \times 10^{-6}/^\circ\text{C}$ and $\alpha_{33}=-21.7 \times 10^{-6}/^\circ\text{C}$).

3.3.2 Piezoelectric properties. The BIBO crystals were found to possess strong piezoelectric properties with longitudinal charge coefficient d_{22} of 40.0 pC/N, double the value of LN crystals ($d_{22} \sim 21 \text{ pC/N}$ [33]). It is believed that the large piezoelectric d_{22} for BIBO crystals is associated with the large polarizability under external stress (dipole moment) and/or the large elastic deformation (higher compliance or smaller stiffness) under electric field. According to the definition of the piezoelectric coefficient $d = (\partial D / \partial T)_E = (\partial S / \partial E)_T$, (D , S , E , T are the electric displacement, strain, electric field and stress, respectively), the variation of the electric displacement ΔD with external stress T under constant electric field E is proportional to the dipole movement, resulting from the polyhedron distortion, while the variation of strain ΔS with electrical field E under constant stress T is closely related to the chemical bonding, associated with the elastic properties. The larger polarizability and/or elastic deformation, the higher piezoelectric coefficient the crystals may possess [35]. Based on discussions on the magnitudes of out-of-center distortion (Δd) for metal-oxygen polyhedrons, referring to the Jahn-Teller effect, the distortion of Bi-O octahedron was calculated and found to be on the order of $\Delta d=1.56 \text{ \AA}$, more than two times that of Nb-O octahedron ($\Delta d=0.64 \text{ \AA}$) in LN crystals, meanwhile, the dipole movement was obtained to be on the order of $0.144 \text{ esu}\cdot\text{cm}/\text{\AA}^3$ for BIBO crystals, three times that for LN crystals ($0.044 \text{ esu}\cdot\text{cm}/\text{\AA}^3$) along the b -axis (polar axis), indicating the larger polarizability of BiBO crystals than LN crystals under the same external stress along b -axis, hence the larger piezoelectric d_{22} for BIBO crystals. On the other hand, the BIBO crystals were revealed to possess strong anisotropy of the elastic properties, with the largest elastic compliance found for s_{22} , being on the order of $85 \text{ pm}^2/\text{N}$, associated with the weak bond strength along the crystallographic b -axis (smaller elastic stiffness c_{22}), which is another important factor accounts for the large piezoelectric d_{22} , though the dielectric permittivity $\epsilon_{22}^T / \epsilon^0$ is low. Again, ultrahigh piezoelectric voltage coefficient g_{22} can be expected due to the large d_{22} and small $\epsilon_{22}^T / \epsilon^0$.

3.4 Temperature dependent behaviours.

3.4.1 Electrical resistivity at elevated temperatures. For piezoelectric sensing applications, the electrical resistivity is critical, especially at elevated temperatures, due to the fact that the lower limiting frequency f_{LL} of a sensor is inversely proportional to the time constant (product of the resistivity and permittivity) [1, 4]. Therefore, the anisotropy of electrical resistivity of BIBO crystals and the temperature dependent

behaviours were investigated, and the results are given in Figure 6.

It was observed that the resistivities ρ along different orientations for BIBO crystals were ranged from $2.0 \times 10^7 \Omega\cdot\text{cm}$ to $2.5 \times 10^8 \Omega\cdot\text{cm}$ at 600°C , where the highest value was achieved for crystal cuts along Y-axis ($\rho_{22}=2.0 \times 10^8 \Omega\cdot\text{cm}$). According to the Arrhenius equation, the activation energies (E_a) for BIBO crystals were calculated and found to be on the order of $1.61 \sim 1.86 \text{ eV}$, slightly higher than that of LN (1.62 eV) crystals along the Y-axis. Of particular interest is that the resistivity of BIBO crystals along Y-axis ($\rho_{22}=2.5 \times 10^8 \Omega\cdot\text{cm}$) is three orders higher than that of LN crystals, being on the order of $1.2 \times 10^5 \Omega\cdot\text{cm}$ at 600°C , together with the high d_{22} , demonstrating the advantages of BIBO crystals for high temperature piezoelectric applications.

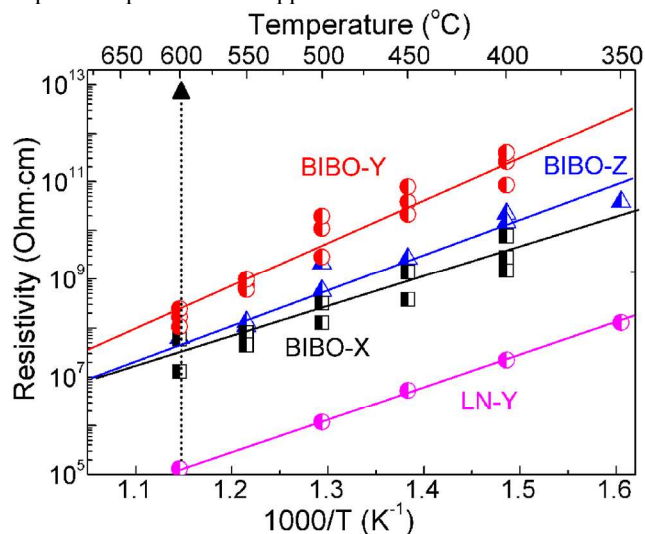


Figure 6 Electrical resistivities of BIBO crystals along physical X-, Y-, and Z-axes, and compared to Y-cut LN crystals.

3.4.2 Temperature dependence of dielectric permittivity.

Variations of dielectric permittivity $\Delta \epsilon / \epsilon_i$ ($i=1, 2$ and 3) as function of temperature up to 600°C were studied for BIBO and compared to LN crystals, as illustrated in Figure 7. Results indicated that the dielectric permittivities $\epsilon_{11}^T / \epsilon^0$ and $\epsilon_{33}^T / \epsilon^0$ for BIBO crystals increased slightly with increasing temperature from 20°C to 600°C , showing positive temperature coefficients of dielectric permittivity ($TC\epsilon$), with variations being on the order of 25% and 18%, respectively, whereas the permittivity $\epsilon_{22}^T / \epsilon^0$ exhibit a negative variation, being -10% over the same temperature range. For comparison, the permittivity $\epsilon_{22}^T / \epsilon^0$ for LN crystals was found to increase dramatically with increasing temperature, showing a large variation of 39%. On the other hand, the dielectric loss for BIBO crystals ($\tan \delta_{22}=15\%$ @ 600°C) was found to be much lower than that of LN crystals ($\tan \delta_{22}=660\%$ @ 600°C). According to the Clausius-Mosotti equation and Harrop chart [37], for BIBO crystal materials with low relative dielectric permittivity ($46 > \epsilon_{ii}^T / \epsilon^0 > 8$) and low dielectric loss ($< 0.1\%$ at RT), the $TC\epsilon$ can be expressed as below,

$$TC\epsilon = C - \alpha \epsilon \quad (10)$$

where C is a constant, α is thermal expansion coefficient and ϵ is the relative dielectric permittivity. Thus, the positive temperature coefficients of $\epsilon_{11}^T / \epsilon^0$ and $\epsilon_{33}^T / \epsilon^0$ (Figure 7) are associated with their low or negative thermal expansion coefficients ($\alpha_{11} = 7.3 \times 10^{-6}$

6°C and $\alpha_{33} = -21.7 \times 10^{-6}/^\circ\text{C}$), while the negative $TC\epsilon$ of $\epsilon_{22}^T/\epsilon^0$ is believed to be associated with the large positive α_{22} value, being on the order of $44.1 \times 10^{-6}/^\circ\text{C}$.

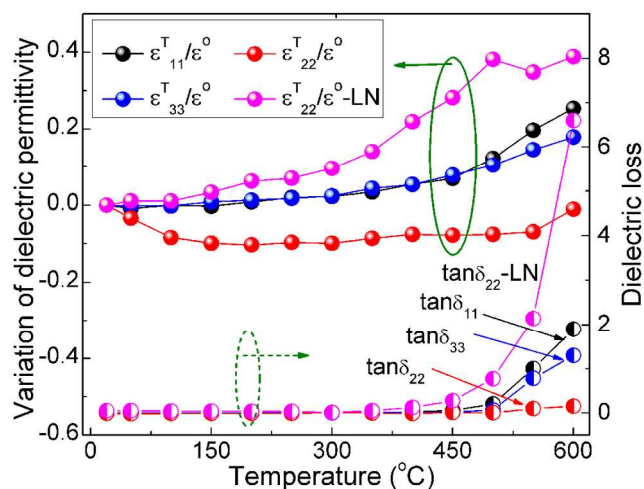


Figure 7 Variation of dielectric permittivity and dielectric loss for BIBO crystals along physical X-, Y-, and Z-axes measured at 1kHz frequency.

3.4.3 Temperature dependence of the electromechanical coupling factors.

The electromechanical coupling factors for various vibration modes, including the transverse, shear and longitudinal vibration modes of BIBO were investigated over the temperature range of 20-600°C and compared to that of LN crystals (Figure 8). It was observed that the face shear electromechanical coupling factors k_{14} and k_{36} for BIBO crystals slightly increase with increasing temperature, with variations being on the order of 13% and 27% over the test temperature range. The thickness shear k_{16} , which was determined to be on the order of 30.9% at room temperature, was found to slightly decrease with increasing temperature, exhibiting a variation of -11%. Interestingly, the BIBO crystals were found to possess high coupling k_{21} , being on the order of 32.1% at RT and 25.4% at 600°C, comparable to those of LN crystals ($k_{21}=30.1\%$ at RT and 26.9% at 600°C), as shown in Figure 8.

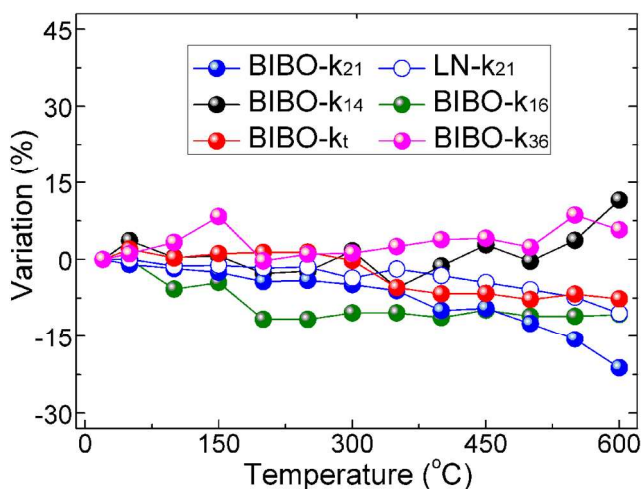


Figure 8 Variation of electromechanical coupling factors for BIBO and LN crystals.

Of particular importance is that BIBO crystals were found to possess minimal temperature variation of thickness coupling factor k_t (measured on Y-plate), being on the order of 40.6% at RT, maintaining the similar value up to 600°C. Taking advantage of the anisotropic electromechanical properties of BIBO crystals, the optimized crystal cuts with high electromechanical coupling and high temperature stability are expected to be designed through crystal cut rotation.

3.4.4 Temperature dependence of piezoelectric coefficients.

Figure 9 presents the variation of selected piezoelectric coefficients (d_{ij} and g_{ij}) as function of temperature for BIBO and LN crystals. It was observed that the face shear piezoelectric d_{14} and d_{36} for BIBO crystals increased with increasing temperature, giving positive variations of 20%-40%. However, the thickness shear piezoelectric coefficient d_{16} , which was determined to be on the order of 13.9 pC/N at room temperature, was observed to decrease with increasing temperature and then slightly increased, with inflection temperature around 200°C, showing an overall variation of -10.5% over the test temperature range. Different from the shear piezoelectric coefficients, the transverse piezoelectric d_{21} , which was determined to be on the order of 16.7 pC/N at RT, was found to exhibit a small negative variation of -11.0%, while the piezoelectric d_{21} for LN crystals shown contrary tendency, with a higher variation being on the order of 15%. In addition, the BIBO crystals were observed to possess high mechanical quality factor Q_m , where Q_{m21} for BIBO crystals was measured to be on the order of 13000 at RT, decreased to 1100 at 600°C, comparable to LN crystals, with mechanical $Q_{m21} = 11000$ and ~ 1000 at RT and 600°C, respectively.

Furthermore, temperature dependence of the piezoelectric voltage coefficients for BIBO (g_{21} and g_{25}) and LN crystals (g_{21}) were investigated, the results are presented in the small inset of Figure 9. It was found that the piezoelectric voltage coefficient g_{21} ($-g_{21}=g_{22}$) for LN crystals was decreased monotonically with increasing temperature, from 29×10^{-3} V·m/N at RT to 23×10^{-3} V·m/N at 600°C, showing a variation of -21%. Comparing to LN crystals, BIBO crystals exhibited not only the large piezoelectric voltage coefficients g_{ij} ($(34-538) \times 10^{-3}$ V·m/N, as presented in Table IV), but also higher temperature stability, where the piezoelectric g_{21} values were found to be on the order of 225×10^{-3} V·m/N at RT and 203×10^{-3} V·m/N at 600°C, giving minimal variation of $\pm 10\%$ over the test temperature range.

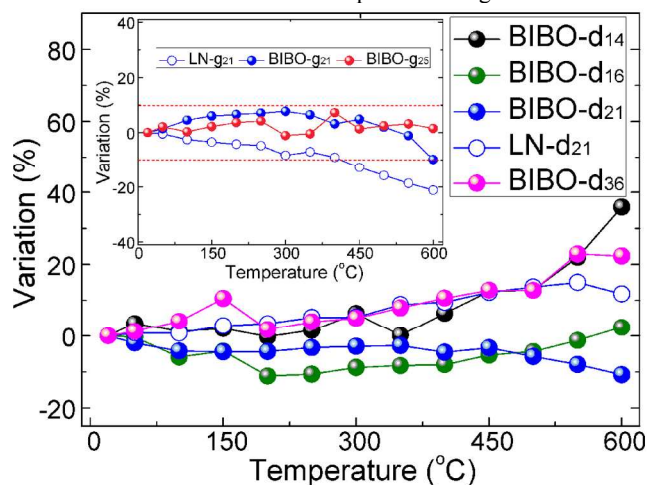


Figure 9 Variation of piezoelectric coefficients for BIBO crystals.

The hydrostatic piezoelectric coefficient d_h is an important parameter for underwater piezoelectric applications. The receiving

sensitivity M ($M=d_h \cdot g_h$) of the piezoelectric element for hydrophone applications is determined by the hydrostatic piezoelectric charge coefficient d_h and voltage coefficient g_h , where the piezoelectric d_h was evaluated by using equation $d_h=d_{21}+d_{22}+d_{23}$ and the voltage coefficient g_h was obtained by using equation $g_h=g_{21}+g_{22}+g_{23}$. It is obtained that BIBO crystal possess large d_h and g_h values, being on the order of 59.2 pm/V and 797×10^{-3} V·m/N, respectively. Table V summarizes the main properties of BIBO crystals and compared to some ferroelectric and non-ferroelectric crystals. It was found that the BIBO crystals possessed low dielectric permittivity, similar to

the reported high temperature piezoelectric crystals GaPO₄, YCOB and GdCOB, while approximate 1% that of PMN-PT and 10% that of LN crystals. Of particular significance is that the BIBO crystals were found to possess high receiving sensitivity M , being on the order of 47.2 pm²/N, 3 times that of commercialized PMN-PT crystals and nearly one order higher than LN crystals. The high piezoelectric (charge and voltage) coefficients and low dielectric loss demonstrate the advantages of the BIBO crystals for hydrophone applications.

Table V Comparison of main properties of BIBO crystals with some ferroelectric and non-ferroelectric crystals.

Crystals		ϵ^r/ϵ^0	$\tan\delta$	k_{eff}	d_h	g_h	$d_h \cdot g_h$
monoclinic	BIBO	8.4	<0.001	0.4	59.2	797	47.2
	TGS[38]	43	-	-	56.7	149	8.4
	YCOB[39]	9.6	<0.001	5.0	-1.9	-24.0	0.05
	GdCOB[40]	9.4	<0.001	6.0	-1.6	-21.5	0.03
trigonal	LN[35]	84	<0.001	0.47	14.5	57	0.8
	GaPO ₄ [1]	6.1	<0.001	0.16	-	-	-
rhombohedral	PMN-PT[7]	4436	0.004	0.88	80	2	0.16

* k_{eff} : %; d_h : pm/V; g_h : 10^{-3} V·m/N; $d_h \cdot g_h$: pm²/N;

D Conclusions

High performance piezoelectric materials with the merits of high resistivity, high piezoelectric coefficient, low dielectric loss and high temperature stability of piezoelectric and electromechanical properties are desired for high temperature sensing applications. In this paper, the electrical resistivity and electro-elastic properties of BIBO crystals were investigated, where the electrical resistivities were found to be on the order of 2.0×10^7 - 2.5×10^8 Ω·cm at 600°C, 2-5 orders higher than LN crystals, with high longitudinal piezoelectric charge coefficients being on the order of $d_{22}=40.0$ pC/N, double the value of LN crystals. Of particular significance is that the BIBO crystals were found to exhibit ultrahigh piezoelectric voltage coefficient, being on the order of $g_{22}=538 \times 10^{-3}$ V·m/N, one order higher than LN crystals ($g_{22}=29 \times 10^{-3}$ V·m/N), and ultrahigh receiving sensitivity M ($d_h \cdot g_h$), being on the order of 47.2 pm²/N, nearly two orders higher than LN crystals. In addition, the BIBO crystals were found to show high temperature stability of electromechanical and piezoelectric properties from RT to 600°C, with minimal variations of $\leq \pm 10\%$. All these properties demonstrate that BIBO crystals are promising for piezoelectric sensing over a broad temperature range.

Acknowledgements

This work was supported by the National Natural Science Foundation of China (Grant Nos. 51202129 and 91022034), and Natural Science Foundation of Shandong Province (ZR2012EMQ004).

Notes and references

^a State Key Laboratory of Crystal Materials, Shandong University, Jinan 250100, P.R. China. Fax: +86 531 88364864; Tel: +86 53188364068; E-mail: zhaoxian@icm.sdu.edu.cn.

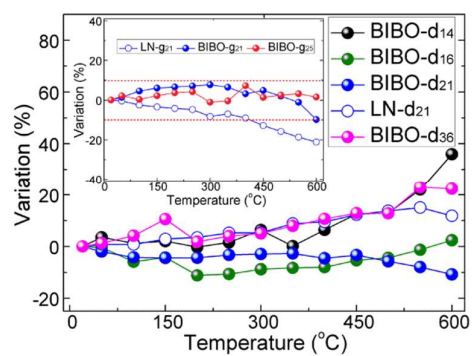
^b School of Chemistry and Chemical Engineering, Shandong University, Jinan 250100, P.R. China.

^c Materials Research Institute, Pennsylvania State University, University Park, PA, 16802, USA. Fax: 1-814-865-7173; Tel: 1-814-863-2639; E-mail: soz1@psu.edu.

^d Key Laboratory of Functional Crystal Materials and Device, Shandong University, Ministry of Education, Jinan 250100, P.R. China.

- S. J. Zhang, and F. P. Yu, *J. Am. Ceram. Soc.*, 2011, **94**, 3153.
- D. Damjanovic, *Curr. Opin. Solid. State Mater. Sci.*, 1998, **3**, 469.
- S. J. Zhang, E. Frantz, R. Xia, W. Everson, J. Randi, D. W. Snyder, and T. R. Shrout, *J. Appl. Phys.*, 2008, **104**, 084103.
- T. R. Shrout, R. Eitel, and C. A. Randall, "High performance, high temperature perovskite piezoelectric ceramics," in *Piezoelectric Materials in Devices*. N. Setter, Ed. Lausanne, Switzerland: EPFL Swiss Federal Institute of Technology, 2002, pp.413-432.
- X. N. Jiang, K. Kim, S. Zhang, J. Johnson and G. Salazar, *Sensors*, 2014, **14**, 144.
- D. Berlincourt, "Piezoelectric Crystals and Ceramics, Chapter 2"; pp. 63-124 in *Ultrasonic Transducer Materials: Piezoelectric Crystals and Ceramics*, Edited by O. E. Mattiat, Plenum, London, 1971.
- S. J. Zhang, F. Li, *J. Appl. Phys.*, 2012, **111**, 031301.
- S. Haussühl, L. Bohatý, P. Becker, *Appl. Phys. A*, 2006, **82**, 495.
- R. T. Smith and F. S. Welsh, *J. Appl. Phys.*, 1971, **42**, 2219.
- F. P. Yu, X. Zhao, L. H. Pan, F. Li, D. R. Yuan, and S. J. Zhang, *J. Phys. D: Appl. Phys.*, 2010, **43**, 165402.
- E. M. Levin, C. L. Mcdaniel, *J. Am. Ceram. Soc.*, 1962, **45**, 355.
- J. Liebertz. *Z. Kristallogr.*, 1982, **158**, 319.
- R. Fröhlich, L. Bohatý, J. Liebertz, *Acta Crystallogr.*, 1984, **C40**, 343.
- R. Cong, J. Zhu, Y. Wang, T. Wang, F. Liao, C. Jin, J. Lin, *CrystEngComm*, 2009, **11**, 1971.
- P. N. Gavryushkin, L. I. Isaenko, A. P. Yelissev, V. A. Gets, and O. S. Il'ina, *Cryst. Growth Des.*, 2012, **12**, 75.
- P. Becket, J. Liebertz, L. Bohatý, *J. Cryst. Growth*, 1999, **203**, 149.
- A. S. Aleksandrovsky, A. D. Vasiliev, A. I. Zaitsev, A. V. Zamkov, *J. Cryst. Growth*, 2008, **310**, 4027.
- Z. P. Wang, B. Teng, K. Fu, X. G. Xu, R. B. Song, C. L. Du, H. D. Jiang, J. Y. Wang, Y. G. Liu, Z. S. Shao, *Opt. Commun.*, 2002, **202**, 217.
- H. Hellwig, J. Liebertz, and L. Bohatý, *Solid State Commun.*, 1999, **109**, 249.
- H. Hellwig, J. Liebertz, and L. Bohatý, *J. Appl. Phys.*, 2000, **88**, 240.
- R. Bechmann, *Phys. Rev.*, 1958, **110**, 1060.
- H. Shimizu, K. Kodama, H. Takeda, T. Nishida, T. Shikida, S. Okamura, and T. Shiosaki, *Jpn. J. Appl. Phys.*, 2004, **43**, 6716.
- H. Shimizu, T. Nishida, H. Takeda, T. Shiosaki, *J. Cryst. Growth*, 2009,

- 311, 916.
- 24 P. Krempf, G. Schleinzer, W. Wallnöfer, *Sensor and Actua. A*, 1997, **61**, 361.
- 25 C. Y. Shen, H. J. Zhang, H. J. Cong, H. H. Yu, J. Y. Wang, and S. J. Zhang, *J. Appl. Phys.*, 2014, **116**, 044106.
- 26 H. Takahashi, M. Hagiwara, H. Noguchi, T. Hoshina, T. Takahashi, N. Kodama, and T. Tsurumi, *Appl. Phys. Lett.*, 2013, **102**, 242907.
- 27 *IEEE Standard on Piezoelectricity*, ANSI/IEEE Standard, **176**, 1987.
- 28 W. P. Mason, *Phys. Rev.*, 1946, **70**, 705.
- 29 R. Fröhlich, L. Bohatý, J. Liebertz, *Acta Cryst.*, 1984, **C40**, 343.
- 30 P. S. Halasyamani, *Chem. Mater.*, 2004, **16**, 3586.
- 31 K. M. Ok, P. S. Halasyamani, D. Casanova, M. Llundell, P. Alemany, and S. Alvarez, *Chem. Mater.*, 2006, **18**, 3176.
- 32 J. J. Zhang, Z. H. Zhang, W. G. Zhang, Q. X. Zheng, Y. X. Sun, C. Q. Zhang, and X. T. Tao, *Chem. Mater.*, 2011, **23**, 3752.
- 33 A. W. Warner, M. Onnw, and G. A. Coquin, *J. Acoust. Soc. Am.*, 1968, **42**, 1223.
- 34 O. Schmidt, S. Gorfman, and U. Pietsch, *Cryst. Res. Technol.*, 2008, **43**, 1126.
- 35 R. E. Newnham, "Properties of Materials: Anisotropy, Symmetry, Structure", Oxford University Press, NY, 2005, pp.58-98.
- 36 V. Petrov, M. Ghotbi, O. Kokabee, A. Esteban-Martin, F. Noack, A. Gaydardzhiev, I. Nikolov, P. Tzankov, I. Buchvarov, K. Miyata, A. Majchrowski, I. V. Kityk, F. Rotermund, E. Michalski, and M. Ebrahim-Zadeh, *Laser & Photon. Rev.*, 2010, **4**, 53.
- 37 A. G. Cockbain, and P. J. Harrop, *Br. J. App. Phys.*, 1968, **1**, 1109.
- 38 Landolt-Bornstein, "Numerical data and functional relationships in science and technology," New Series Group III, Springer-Verlag Heidelberg, New-York, **11**, 1979.
- 39 F. P. Yu, S. Hou, S. J. Zhang, Q. M. Lu, and X. Zhao, *Phys. Status. Solidi A*, 2014, **3**, 574.
- 40 F. P. Yu, X. L. Duan, S. J. Zhang, Q. M. Lu, and X. Zhao, *Crystals*, 2014, **4**, 241.



BiB_3O_6 crystals possess large piezoelectric coefficients and high temperature stability of piezoelectric properties, promising for piezoelectric sensor applications.